BIOCHEMISTRY
including biophysical chemistry & molecular biology

Article

pubs.acs.org/biochemistry

Open Access on 07/16/2015

The Middle X Residue Influences Cotranslational N-Glycosylation Consensus Site Skipping

Heidi L. H. Malaby and William R. Kobertz*

Department of Biochemistry and Molecular Pharmacology and Programs in Neuroscience and Chemical Biology, University of Massachusetts Medical School, 364 Plantation Street, Worcester, Massachusetts 01605-2324, United States

Supporting Information

ABSTRACT: Asparagine (N)-linked glycosylation is essential for efficient protein folding in the endoplasmic reticulum (ER) and anterograde trafficking through the secretory pathway. N-Glycans are attached to nascent polypeptides at consensus sites, N-X-T/S (X ≠ P), by one of two enzymatic isoforms of the oligosaccharyltransferase (OST), STT3A or STT3B. Here, we examined the effect of the consensus site X and hydroxyl residue on the distributions of co- and post-translational N-glycosylation of a type I transmembrane glycopeptide scaffold. Using rapid radioactive pulse−chase experiments to resolve co-translational (STT3A) and post-translational (STT3B) events, we determined that NXS consensus sites containing large hydrophobic and negatively charged middle residues are frequently skipped by STT3A during protein translation. Post-translational modification of the cotranslationally skipped sites by STT3B was similarly hindered by the middle X residue, resulting in hypoglycosylation of NXS sites containing large hydrophobic and negatively charged side chains. In contrast, NXT consensus sites (barring NWT) were efficiently modified by the cotranslational machinery, reducing STT3B's role in modifying consensus sites skipped during protein translation. A strong correlation between cotranslational N-glycosylation efficiency and the rate of post-translational N-glycosylation was determined, showing that the OST STT3A and STT3B isoforms are similarly influenced by the hydroxyl and middle X consensus site residues. Substituting various middle X residues into an OST eubacterial homologous structure revealed that small and polar consensus site X residues fit well in the peptide binding site whereas large hydrophobic and negatively charged residues were harder to accommodate, indicating conserved enzymatic mechanisms for the mammalian OST isoforms.

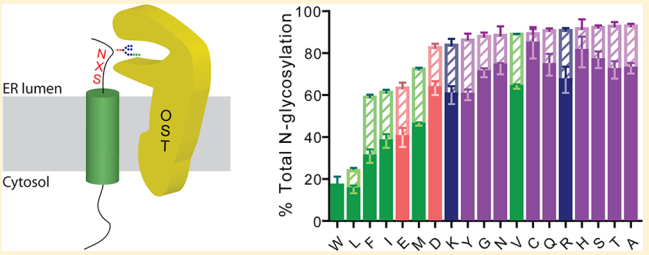

The vast majority of secretory and integral membrane proteins acquire asparagine (N)-linked glycans during biosynthesis to ensure proper folding, assembly, and trafficking out of the endoplasmic reticulum (ER). The covalent attachment of the 14-sugar oligosaccharide to a nascent chain at an N-X-T/S consensus site, where X can be any amino acid except proline, is catalyzed by the oligosaccharyltransferase (OST).[1,2] This ER luminal membrane protein complex is composed of seven or eight individual subunits in eukaryotes and undergoes a vast array of diverse functions, including positioning the lipid-linked oligosaccharide donor and scanning and positioning a peptide chain for N-glycosylation. N-Glycans can be added cotranslationally to the growing peptide while it is inserted into the ER via the translocon (Sec61 complex)[3] or post-translationally after the peptide is fully synthesized.[3−7]

OST catalytic subunit STT3 is the only domain of the complex that is conserved from eukaryotes to eubacteria.[8] High-resolution structures have been determined for the bacterial and aracheal OST STT3 homologues.[9,10] Despite having sequences that are only 20% identical, these structures are remarkably similar. For vertebrates, plants, and most insects, there are two known eukaryotic isoforms of the OST catalytic subunit designated STT3A and STT3B. Utilizing kinetic assays, the OST STT3A isoform has been shown to predominantly perform cotranslational N-glycosylation while the OST STT3B isoform preferentially N-glycosylates peptides post-translationally.[5−7] Intriguingly, STT3B was found to perform cotranslational N-glycosylation if STT3A is depleted, but STT3A does not perform post-translational N-glycosylation in the absence of STT3B,[5] indicating affinity differences between these different OST isoform complexes. While STT3A and STT3B isoforms are ∼60% conserved, their N-glycosylation kinetics and variations in peptide sequence recognition are not well understood.

The primary sequence context of an N-linked glycosylation consensus site has been known to affect OST N-glycan attachment efficiency, including the consensus site hydroxyl and middle residues,[11−14] specific residues upstream or downstream of or the residue immediately following the consensus site,[15−17] and the proximity of a consensus site to other consensus sites[18] and the C-terminus.[7] Although several molecular factors affect N-glycosylation efficiency, particularly for NXS consensus sites that have been shown to be more

Received: June 3, 2014
Revised: July 15, 2014
Published: July 16, 2014

   dx.doi.org/10.1021/bi500681p | *Biochemistry* 2014, 53, 4884−4893

sensitive to sequence elements than NXT sites,[13,14] a plausible mechanism for this disparity has not been determined, nor have the biophysical ramifications of these differences been characterized in the context of the OST STT3A and STT3B isoforms.

Here, we use a type I transmembrane glycopeptide (KCNE2) as a scaffold to determine the co- and post-translational N-glycosylation distributions for all amino acids in the middle residue of an NXS consensus site. We found that middle residues with small hydrophobic, positively charged, and polar side chains are efficiently cotranslationally N-glycosylated. In contrast, consensus sites with bulky hydrophobic or negatively charged middle X residues are often skipped during protein translation, resulting in a higher percentage of N-glycans being added after protein synthesis. Similar to water-soluble and type II transmembrane proteins,[5,7] the STT3A and STT3B isoforms were primarily responsible for co- and post-translational N-glycosylation of type I transmembrane peptides, respectively. By comparing the amount of cotranslational N-glycosylation to the rate of post-translational N-glycosylation, we found that STT3A and STT3B isoforms modify NXS sites at similar efficiencies, suggesting that these isoforms have a conserved catalytic mechanism that is influenced by the side chain of the middle residue in the consensus sequence.

EXPERIMENTAL PROCEDURES

Cloning and Plasmids. Human KCNE2 and KCNE4 were cloned into the pcDNA3.1$^{(-)}$ vector such that five additional methionine residues and an HA tag (YPYDVPDYA) were added to the C-terminus of each KCNE peptide.[19,20] The second N-glycosylation consensus site was removed in KCNE2 by mutation to glutamine (N29Q). Mutations for creating different X residues in NXS or NXT sites were introduced using traditional polymerase chain reaction cassette mutagenesis (Syzygy Biotech Taq 2x MeanGreen Master Mix) between the 5′ *Kpn*I and 3′ *Bgl*II sites. All constructs were confirmed by DNA sequencing the entire gene.

Cell Culture and Plasmid Transfection. Chinese hamster ovary K1 (CHO) cells were maintained in Gibco-F12K Nutrient Mixture, Kaighn's Modification (with L-glutamine) medium, supplemented with 10% FBS (Sigma) and 1% penicillin/streptomycin. Cells were passaged using 0.5% Trypsin-EDTA and plated onto 35 or 100 mm dishes at 80% confluency for Western blots or pulse−chase experiments, respectively. After 24 h, the cells (35 or 100 mm dishes) were transiently transfected with a mixture of 1.5 or 3.0 μg of KCNE DNA and 8 or 16 μL of Lipofectamine in 1 or 2 mL of OptiMem, respectively. After 6 h at 37 °C, the transfection cocktail was removed and F12K medium with supplements was added.

siRNA Transfection for Pulse−Chase and Western Blot Experiments. Cells at 80% confluency were transiently transfected with a mixture of small interfering RNA (siRNA): scrambled **A**, GAGAACUAACGCAAGAGAAdTdT; scrambled **B**, GAAGGCACCGGUUAUUAGUdTdT; STT3A, GAAGACACAUCAAGGAGAAdTdT; STT3B, GGACUACUCUGGUGGAUAAdTdT. The different siRNA mixtures (100 nmol of **A**; 150 nmol of **B**) were incubated (5 min) before being combined with 16 μL of Lipofectamine 2000 in OptiMem (400 μL) for 30 min and then diluted into 2 mL of OptiMem. After 6 h at 37 °C, the transfection cocktail was removed and 2 mL of F12K medium with supplements was added, and the cells were incubated for 40−45 h. Another round of siRNA transfection was performed as described above with the addition of 3 μg of E2 DNA (NFT or NFS) to the transfection cocktail. After 6 h at 37 °C, the transfection cocktail was removed and 2 mL of F12K medium with supplements was added, and the cells were incubated for an additional 40−45 h.

Pulse−Chase Assays and Cell Lysis. Pulse−chase experiments and cell lysis were performed as previously described.[20] Briefly, transfected cells were washed with PBS and incubated for 35 min at 37 °C in Gibco DMEM High Glucose Media (4.5 g/L D-glucose, lacking L-methionine and L-cysteine), supplemented with 10% FBS, 1% Pen Strep, and 2 mM L-glutamine. The medium was removed, and the cells were incubated at 37 °C for 2 min in DMEM High Glucose Media containing 100 μCi/mL EasyTag EXPRESS [^{35}S] Protein Labeling Mix (PerkinElmer). The radioactive medium was removed, and the cells washed with PBS and chased with F12K medium for 3, 6, 9, or 12 min at 37 °C. The cells were then washed with PBS and lysed with 750 μL of low-salt lysis buffer [50 mM Tris-HCl (pH 7.4), 150 mM NaCl, 20 mM NaF, 10 mM Na_3VO_4, 1% NP-40, and 1% CHAPS], which was supplemented with protease inhibitors: 1 mM phenylmethanesulfonyl fluoride (PMSF) and 1 μg/mL leupeptin, 1 μg/mL pepstatin, and 1 μg/mL aprotinin (LPA). Cells were lysed for 30 min while being vigorously shaken at 4 °C, and the cell debris was scraped and pelleted at 14000 rpm for 10 min at room temperature.

Radioimmunoprecipitation and Electrophoresis. Radioimmunoprecipitation and electrophoresis for pulse−chase experiments were performed as previously described.[20] Briefly, Protein G agarose beads (Pierce) were prepared by being washed in low-salt lysis buffer. After the cell debris had been pelleted, the supernatant was precleared with 50 μL of beads for 2 h at 4 °C. The beads were then spun down, and the supernatant was transferred to new tubes containing 25 μL of beads preincubated with 1 μL of monoclonal anti-HA antibody (Sigma). After an overnight incubation at 4 °C, the beads were pelleted, the supernatant was removed, and the beads were subjected to three washes of low-salt lysis buffer, one wash of high-salt buffer [50 mM Tris-HCl (pH 7.4), 500 mM NaCl, 1% NP-40, 1% CHAPS, 20 mM NaF, and 10 mM Na_3VO_4], and a final wash with low-salt lysis buffer. For enzymatic deglycosylation assays, 1 μL of Endo H_f (New England Biolabs) was added to beads in 50 μL of low-salt lysis buffer and incubated at 37 °C for 1 h. Peptides were eluted from the beads with 100 mM DTT and 2× SDS gel loading buffer at 55 °C for 15 min. Samples were analyzed by 15% sodium dodecyl sulfate−polyacrylamide gel electrophoresis (SDS−PAGE), and the gels were dehydrated for 1 h in a 30% ethanol/2% glycerol solution. Gels were dried for 2 h at 80 °C, applied to a photostimulable phosphor plate, and analyzed for photostimulated luminescence with a Typhoon FLA-9000 phosphoimager after 14−42 days.

Western Blots. Cells were washed in PBS (3 × 750 μL) and lysed with RIPA buffer [10 mM Tris-HCl (pH 7.4), 140 mM NaCl, 1 mM EDTA (pH 7.4), 1% Triton X-100, 0.1% SDS, and 1% sodium deoxycholate], supplemented with protease inhibitors (PMSF and LPA). After the sample had vigorously shaken for 30 min at 4 °C, the cell debris was scraped and pelleted at 14000 rpm for 10 min at room temperature. The total protein in each sample was determined by a bicinchonimic acid (BCA) assay and 60 μg of protein utilized for electrophoresis. Samples were prepared by adding 100 mM DTT and 2× SDS gel loading buffer to the lysis sample to yield a total volume of 50 μL. Samples were analyzed

dx.doi.org/10.1021/bi500681p | *Biochemistry* 2014, 53, 4884−4893

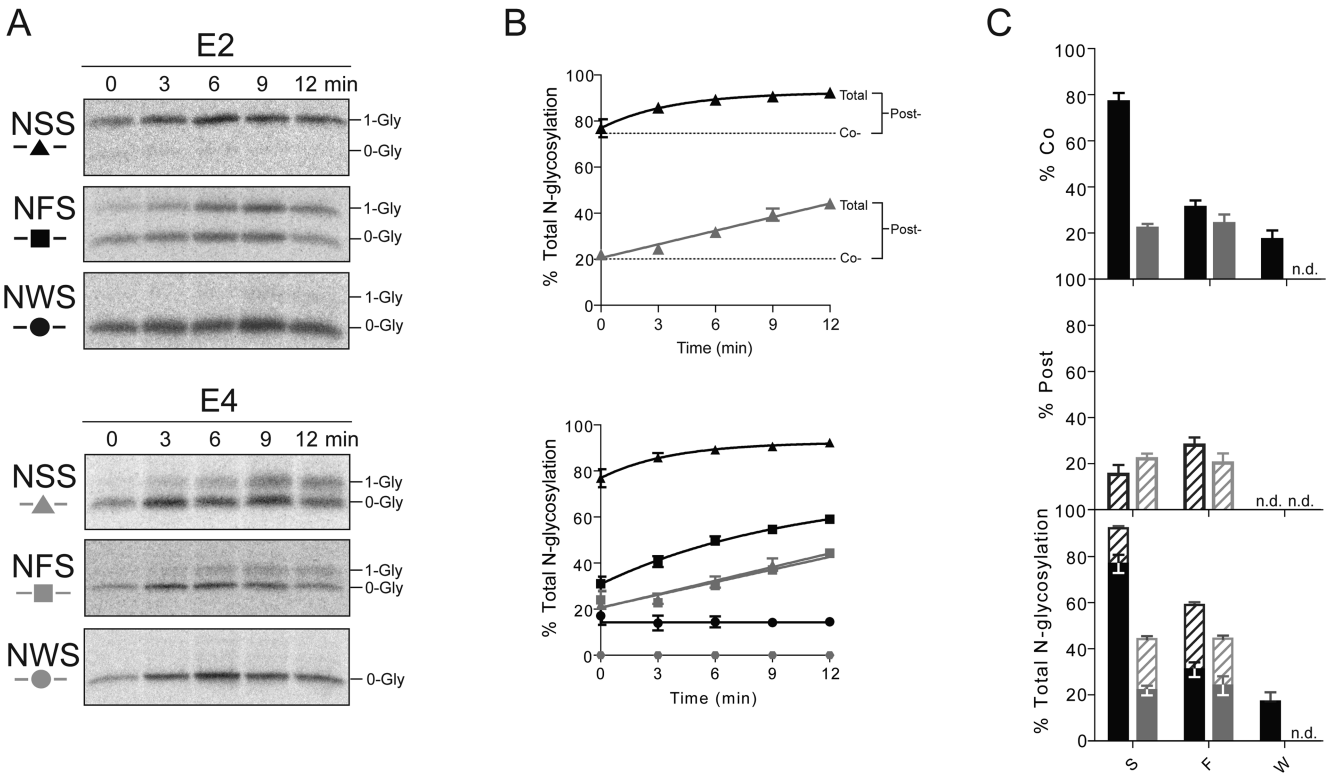

Figure 1. Middle X residue in NXS consensus sites alters the distribution of co- and post-translational N-glycosylation of type I transmembrane peptides. (A) Representative fluorographs from pulse−chase experiments of E2 and E4 constructs containing a single NXS consensus site (E2, N6; E4, N8). Glycosylated (1-Gly) and unglycosylated (0-Gly) species are labeled for the NSS, NFS, and NWS consensus sites. (B) The top panel is a plot of total N-glycosylation for the NSS sites in E2 (black triangles) and E4 (gray triangles). The co- and post-translational N-glycosylation distributions are demarcated. The bottom panel is a kinetic comparison of all six NXS sites: E2 NSS (black triangles), E4 NSS (gray triangles), E2 NFS (black squares), E4 NFS (gray squares), E2 NWS (black circles), and E4 NWS (gray circles). (C) Quantification of the cotranslational (solid bars), post-translational (hatched bars), and total N-glycosylation for the E2 (black) and E4 (gray) consensus sites. The error bars show the standard error of the mean for three experiments; n.d. means not detected. The errors in the combined bar graph are denoted as follows: cotranslational (middle bar, up), post-translational (middle bar, down), and total N-glycosylation (top bar, up).

by 8% SDS−PAGE, transferred to a nitrocellulose membrane, and incubated for 30 min in blocking buffer [5% nonfat dry milk in Tris-buffered saline containing 0.2% Tween 20 (western wash buffer)]. STT3 primary antibodies were obtained from R. Gilmore,[5] diluted in blocking buffer (1:2500 for STT3A or 1:6000 for STT3B), and allowed to incubate overnight at 4 °C. Membranes were washed in western wash buffer (3 × 6 mL) for 5 min each and incubated for 45 min at room temperature with the rabbit anti-STT3 antibody (1:4000 for STT3A or 1:10000 for STT3B)[5] in western blocking buffer. After being washed (3 × 6 mL) with western wash buffer, the membrane was incubated (5 min) with SuperSignal West Dura Extended Duration Substrate (Pierce); the chemiluminescence was captured using an LAS-3000 CCD camera and quantified by Multi Gauge software (Fujifilm).

Data Analysis. All signals were quantified using Image Gauge software (Fujifilm).[20] The percentage of glycosylation for every time point was determined by dividing the signal of the glycosylated species by the total amount of signal (0-Gly + 1-Gly). The 12 min time point served as the percent total N-glycosylation for every NXS and NXT construct. To determine the cotranslational N-glycosylation contribution for each construct, we divided the percent N-glycosylated at 0 min by the percent N-glycosylated at 12 min. Our simplified calculation for cotranslational N-glycosylation assumes that the peptide substrates are fully synthesized before the 3 min time point[21] and that the observable rates for co- and post-translational N-glycosylation are substantially different for this class of peptides.[19] To calculate the post-translational N-glycosylation contribution, we subtracted the cotranslational component (0 min) from the total N-glycosylation (12 min) and divided it by the total N-glycosylation (12 min). The percent total N-glycosylation bar graphs show the cotranslational (solid) and post-translational (slashed) contributions with the errors between the interface representing the errors associated with cotranslation (up error bar) and post-translation (down error bar). Post-translational N-glycosylation kinetic rates (k) were determined by fitting the data to the single-exponential equation $y = y_0 + (\text{plateau} - y_0)(1 - e^{-kx})$.

PyMOL Model Generation. Middle X residue models were generated from the PglB crystal structure [Protein Data Bank (PDB) entry 3RCE]. Surface representations and stick models are shown for PglB residues, and stick and sphere models are shown for peptide residues. To ascertain the middle X residue fit into the peptide binding site, the crystallized X residue (alanine) was mutagenized to serine (three rotamers, no steric clash), threonine (two rotamers, no steric clash), lysine (17 rotamers, four with steric clash), glutamine (11 rotamers, three with steric clash), arginine (19 rotamers, six with steric clash), cysteine (three rotamers, one with steric clash), valine (three rotamers, one with steric clash), asparagine (12 rotamers, four with steric clash), aspartic acid (nine rotamers, three with steric clash), methionine (nine rotamers, three with steric clash), glutamic acid (14 rotamers, six with steric clash), isoleucine

dx.doi.org/10.1021/bi500681p | Biochemistry 2014, 53, 4884−4893

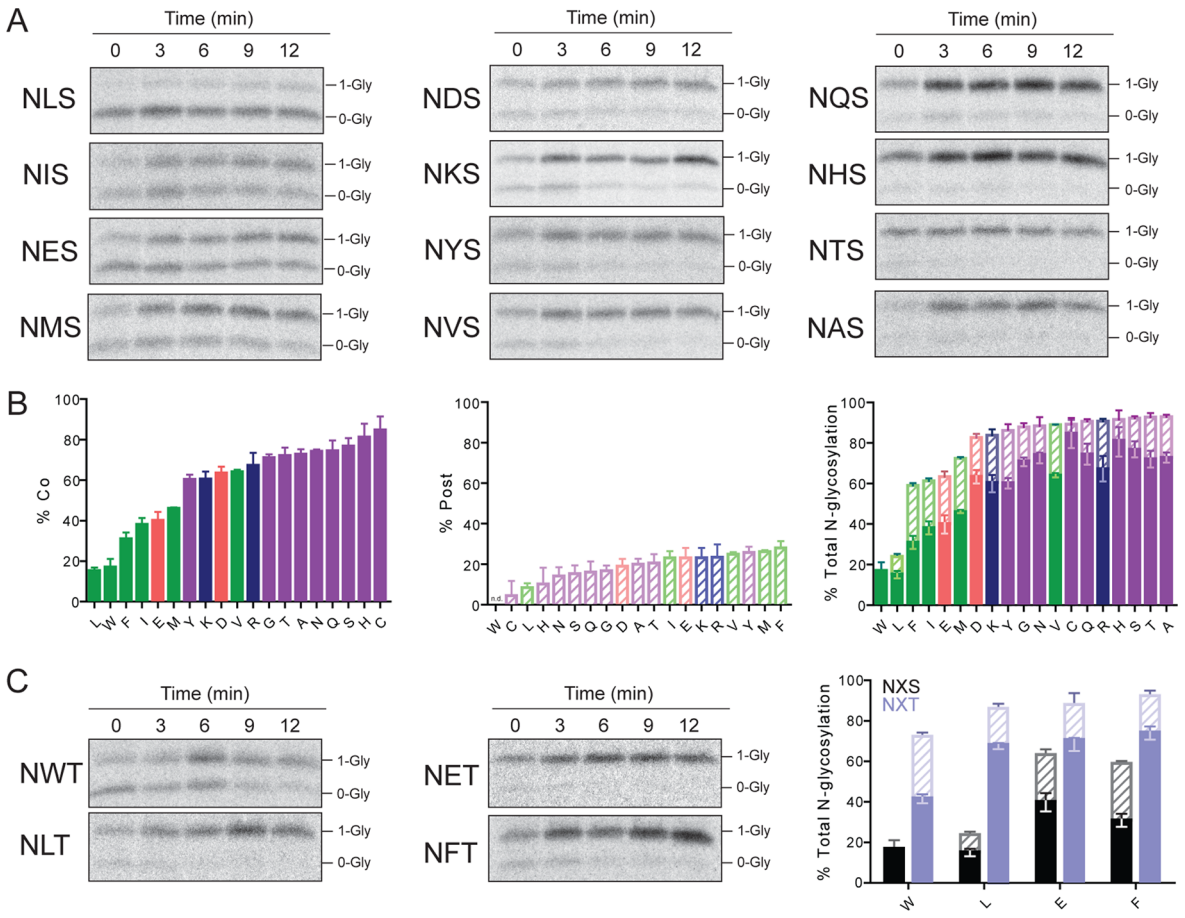

Figure 2. Large hydrophobic and negatively charged middle X residues in NXS but not NXT sites hinder cotranslational N-glycosylation. (A) Representative fluorographs from pulse−chase experiments for all middle X residues (except proline) in an E2 NXS consensus site. Glycosylated (1-Gly) and unglycosylated (0-Gly) species are labeled. Fluorographs for NGS, NNS, NCS, and NRS are shown in Figure 1B of the Supporting Information. (B) Bar graphs of cotranslational (solid), post-translational (hatched), and total N-glycosylation for the consensus site X residues. Polar and small hydrophobic amino acids are colored purple, large hydrophobic amino acids green, and positively and negatively charged amino acids blue and red, respectively. (C) Representative fluorographs (left and middle) from pulse−chase experiments for middle X residues in NXT sites. Glycosylated (1-Gly) and unglycosylated (0-Gly) species are labeled. Bar graph comparison (right) of cotranslational (solid), post-translational (hatched), and total N-glycosylation for consensus site X residues in NXS (black) and NXT (blue) sites. All error bars show the standard error of the mean for three experiments; n.d. means not detected. The errors in the combined bar graph are denoted as follows: cotranslational (middle bar, up), post-translational (middle bar, down), and total N-glycosylation (top bar, up).

(two rotamers, one with steric clash), leucine (five rotamers, four with steric clash), histidine (seven rotamers, seven with steric clash), phenylalanine (four rotamers, four with steric clash), tyrosine (four rotamers, four with steric clash), and tryptophan (nine rotamers, nine with steric clash). Rotamers shown in Figure 5 had either no steric clash or the smallest amount of steric clash (Trp).

RESULTS

To determine the effects of the middle X residue on the kinetics of N-glycosylation, we needed to identify a kinetically sensitive consensus site that would allow for the highest resolution of co- and post-translational N-glycosylation events using rapid metabolic pulse−chase experiments.[5,19] Previously, we have shown that members of the KCNE family (E1−E5) of type I transmembrane peptides possess several consensus sites where the N-glycosylation kinetics can be flipped from co- to post-translational (and vice versa) by simply switching the hydroxyl residue in the consensus site.[19,20] We chose E2 and E4 as test substrates because they incorporate more ^{35}S radiolabel and the attachment of the N-glycan to these peptides depends on the consensus site hydroxyl group.[20] Because N-glycosylation efficiencies of NXS consensus sites are more sensitive to the middle X residue,[13] we settled on E2 and E4 constructs that had a single N-terminal NXS consensus site, which (i) simplifies the kinetic measurements and (ii) eliminates any cooperativity caused by the presence of multiple consensus sites.[20]

On the basis of previous consensus site X residue efficiencies,[13] we compared the N-glycosylation kinetics at three sites that are efficiently (NSS), moderately (NFS), and poorly (NWS) glycosylated. Figure 1A shows the unglycosylated (0-Gly) and singly glycosylated (1-Gly) species for each construct, which were confirmed by endoglycosidase H digestion (Figure 1A of the Supporting Information). The percentage of glycosylated protein was then calculated by normalizing the 1-Gly intensity to the total protein for each time point and graphed as shown in Figure 1B. To determine the co- and post-translational components, we exploited the significant kinetic difference between co- and post-translational N-glycosylation[5] and used a simplified convention in which co- is defined as the glycosylated protein present at the start of the

dx.doi.org/10.1021/bi500681p | Biochemistry 2014, 53, 4884−4893

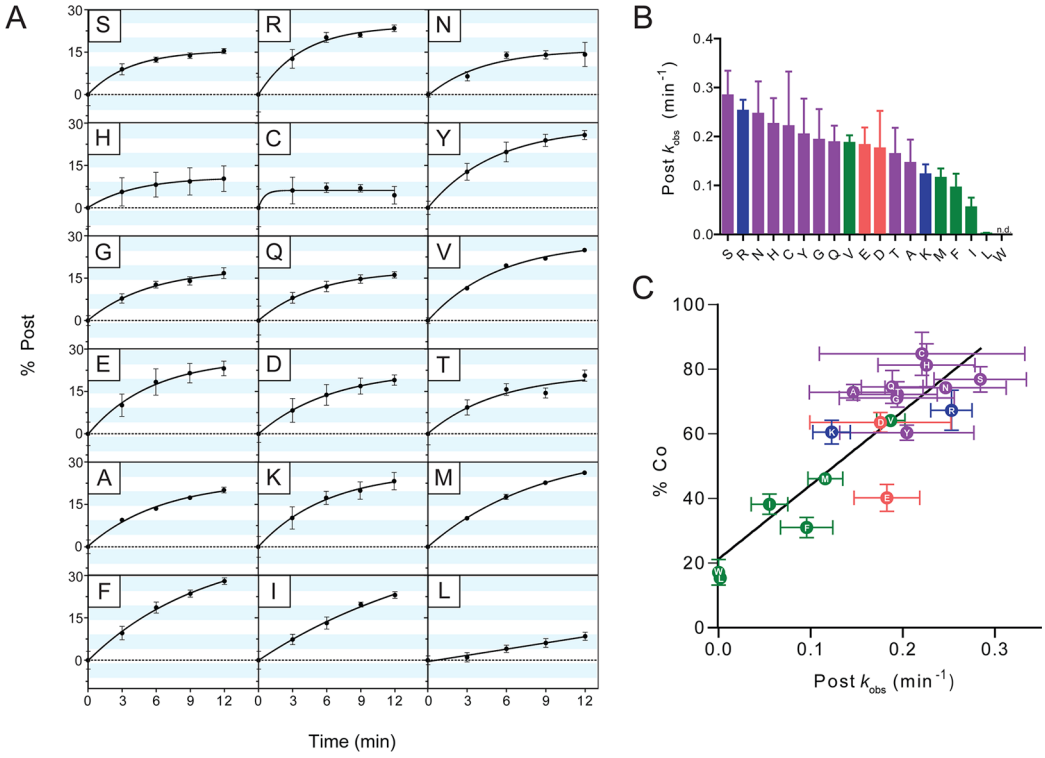

Figure 3. Post-translational N-glycosylation rates of NXS consensus sites mirror cotranslational N-glycosylation efficiency. (A) Post-translational N-glycosylation kinetics for each NXS consensus site except tryptophan. Data are fit to a single-exponential equation, and the rates are plotted in panel B. (B) Polar and small hydrophobic amino acids are colored purple, large hydrophobic amino acids green, and positively and negatively charged amino acids blue and red, respectively. (C) Correlation plot of co- and post-translational N-glycosylation (R^2 = 0.76). The coloring is the same as in panel B. All error bars show the standard error of the mean from three experiments; n.d. means not detected.

chase period (0 min) and post- is defined as the increase in glycosylation measured over the experimental time course (Figure 1B, top). Using these conventions, we compared the amount of cotranslational, post-translational, and total N-glycosylation for each NXS construct (Figure 1C). This initial comparison demonstrated that the middle X residue strongly influences the kinetics of attachment of the N-glycan to NXS consensus sites.

Because the test NXS consensus sites in the E2 construct displayed the widest range of cotranslational, post-translational, and total N-glycosylation, we subsequently used this E2 construct to compare the N-glycosylation kinetics for all middle X residues (except proline) (Figure 2 and Figure 1B of the Supporting Information). The cotranslational, post-translational, and total N-glycosylation quantifications are shown for each construct in Figure 2B. Cotranslational N-glycosylation ranged from ∼20 to 85% with the most efficient NXS consensus sites containing either small (polar and hydrophobic) or positively charged middle X residues (Figure 2B, left). Conversely, NXS consensus sites with either large hydrophobic or glutamic acid middle X residues were poorly (<50%) cotranslationally N-glycosylated. In agreement with the temporal divisions between co- and post-translational N-glycosylation, the largest post-translational contributors to total N-glycosylation, for the most part, were the NXS consensus sites that were skipped during protein translation (Figure 2B, middle). NWS and NLS were the two exceptions, as these were bad substrates for both co- and post-translational N-glycosylation. This inverse relationship between co- and post-translational N-glycosylation likely arises from the availability of a larger pool of unglycosylated substrates available for post-translational N-glycosylation. Nonetheless, under these experimental conditions, post-translational N-glycosylation did not fully compensate for NXS consensus sites containing middle F, I, E, or M residues, keeping the total N-glycosylation efficiency for these consensus sites significantly below the predominately cotranslational consensus sites (Figure 2B, right).

In contrast to NXS consensus sites, previous studies have shown that NXT sites are efficiently N-glycosylated regardless of the middle X residue.[7,20] Therefore, we converted the most inefficient NXS sites into NXT sites to determine which kinetic component of N-glycosylation was responsible for the improved N-glycan attachment. As expected, the N-glycosylation efficiency for all four NXT sites was significantly improved compared to those of their NXS counterparts (Figure 2C). Dissection of the kinetic components of N-glycosylation revealed that the increase in the extent of attachment of N-glycans to these NXT sites occurred primarily during translation. For NWT consensus sites, post-translational N-glycosylation was also markedly improved. Thus, attachment of N-glycans to NXT sites is unaffected by the middle X residue because these sites are efficiently cotranslationally glycosylated.

To determine the influence of the middle X residue on post-translational N-glycosylation kinetics, we fit the pulse−chase data for each NXS consensus site to a single-exponential equation and compared the observed post-translational N-glycosylation rates to cotranslational N-glycosylation efficiency (Figure 3). Similar to cotranslational N-glycosylation efficiency (Figure 2B), the kinetics of post-translational N-glycosylation depended on the middle X residue, where large hydrophobic residues had the slowest rates of post-translational N-

dx.doi.org/10.1021/bi500681p | *Biochemistry* 2014, 53, 4884−4893

glycosylation (Figure 3B and Table 1). To compare co- and post-translational N-glycosylation for each middle residue, we

Table 1. Consensus Site Middle Residue N-Glycosylation[a]

	% co	% post	% total	post k_{obs} (min^{-1})
		E2 NXS		
W	17 ± 4	nd	17 ± 4	nd
L	15 ± 2	9 ± 2	24 ± 1	–
F	31 ± 3	28 ± 3	59 ± 1	0.10 ± 0.03
I	38 ± 3	23 ± 3	61 ± 1	0.06 ± 0.02
E	40 ± 4	23 ± 5	63 ± 3	0.18 ± 0.04
M	46 ± 1	26 ± 1	72 ± 1	0.12 ± 0.02
D	64 ± 3	19 ± 4	83 ± 2	0.18 ± 0.08
K	61 ± 4	23 ± 5	84 ± 3	0.12 ± 0.02
Y	60 ± 2	26 ± 3	87 ± 3	0.21 ± 0.07
G	71 ± 2	17 ± 3	88 ± 2	0.19 ± 0.06
N	74 ± 1	14 ± 4	89 ± 4	0.25 ± 0.07
V	64 ± 1	25 ± 1	89 ± 1	0.19 ± 0.02
C	85 ± 7	5 ± 7	89 ± 3	0.22 ± 0.11
Q	75 ± 5	16 ± 5	91 ± 1	0.19 ± 0.03
R	67 ± 6	24 ± 6	91 ± 1	0.25 ± 0.02
H	81 ± 7	10 ± 8	92 ± 5	0.23 ± 0.05
S	77 ± 4	15 ± 4	92 ± 1	0.28 ± 0.05
T	72 ± 4	21 ± 4	93 ± 2	0.20 ± 0.04
A	73 ± 2	20 ± 3	93 ± 1	0.15 ± 0.05
		E2 NXT		
W	42 ± 2[b]	31 ± 3[b]	72 ± 2[b]	0.08 ± 0.03
L	68 ± 1[b]	18 ± 2	86 ± 2[b]	0.28 ± 0.05
E	71 ± 1[b]	17 ± 6	88 ± 6[b]	0.43 ± 0.14[b]
F	74 ± 3[b]	18 ± 4	93 ± 3[b]	0.20 ± 0.01
		E4 NXS		
W	nd	nd	nd	nd
F	24 ± 4	20 ± 4	44 ± 1	–
S	22 ± 2	22 ± 2	44 ± 1	–

[a]Cotranslational, post-translational, total N-glycosylation, and post-translational rates shown for each E2 or E4 NXS or NXT middle residue consensus site. The percentages of co- and post-translational N-glycosylation were determined as described in Experimental Procedures. Values are means ± the standard error of the mean for three pulse–chase experiments. [b]$p < 0.05$ (two-way analysis of variance; NXT sites compared to their equivalent NXS sites). This indicates significance by Tukey's multiple-comparison test (E2 NXT values compared to equivalent E2 NXS sites). Post-translational rates were averaged from independent pulse–chase experiments in which the association rate (k_{obs}) was determined by fitting the data to a single-exponential equation; nd means not detected. A dash means $k_{obs} < 0.05$, indicating post-translational rates were too slow to accurately fit.

plotted the observed post-translational N-glycosylation rate constant (k_{obs}) versus the percentage of cotranslational N-glycosylation (Figure 3C). Despite the large errors associated with the inability to control substrate, enzyme, and competitor concentrations as well as the rate of protein degradation in living cells, these N-glycan attachment data ($R^2 = 0.76$) suggest that the OST STT3 isoforms associated with co- and post-translational N-glycosylation operate at similar efficiencies and by similar mechanisms.

Previous studies with water-soluble and type II transmembrane peptides have shown that as the protein is threaded into the ER lumen the OST STT3A isoform performs cotranslational N-glycosylation whereas the STT3B isoform is responsible for post-translational N-glycosylation.[5,7] Because the N-terminus of type I transmembrane peptides without a cleavable signal sequence is inserted into the ER en masse, we wanted to ensure that OST STT3 enzyme specificity was not affected by the ER insertion mechanism. To identify the OST STT3 isoform(s) associated with co- and post-translational N-glycosylation of the NXS and NXT substrates, we specifically reduced the protein levels of either STT3 isoform or both using small interfering RNAs (siRNAs) and then compared the N-glycosylation kinetics for NXS and NXT sites containing a middle phenylalanine residue. Because the STT3 proteins are relatively stable and do not turn over quickly, we performed two sequential siRNA transfections (Experimental Procedures) as previously described for STT3 isoform-specific knockdowns in HeLa cells.[5,7] This sequential knockdown reduced the levels of STT3A protein 74 ± 3% when STT3A was targeted and 57 ± 4% when STT3A and STT3B were targeted. A similar reduction in the level of STT3B protein (63 ± 6 and 70 ± 2%) was observed when siRNAs targeted to STT3B were used and siRNAs targeted to STT3B and STT3A were used, respectively. Scrambled sequences or siRNAs for the opposite isoform had no significant effect on STT3 protein levels (Figure 2 of the Supporting Information).

Using this siRNA transfection strategy, cells expressing the NFS substrate were pulsed with ^{35}S-labeled amino acids and chased for 0–12 minutes (Figure 4A, left). For the NFS site, reduction of either STT3A or STT3B protein did not affect cotranslational N-glycosylation (Figure 4B, left). The lack of an effect was expected because previous studies have shown that the STT3B isoform performs cotranslational N-glycosylation when STT3A protein levels are reduced.[5] Simultaneous knockdown of STT3A and STT3B (Figure 4A,B) confirmed that both OST isoforms must be reduced to significantly reduce cotranslational N-glycosylation. In contrast to cotranslational N-glycosylation, post-translational N-glycosylation of the NFS site was not detectable by selectively knocking down the STT3B isoform compared to scrambled and STT3A controls (Figure 4B, left).

We then challenged the robustness of the isoform-specific siRNA experiments by examining the more efficiently N-glycosylated NFT site (Figure 4, right panels). Similar to the NFS site, reduction of STT3A protein levels had no effect on cotranslational N-glycosylation; reduction of STT3B protein levels significantly reduced post-translational N-glycosylation, and reduction of both isoforms substantially reduced both co- and post-translational N-glycosylation (Figure 4B, right panels). Surprisingly, knockdown of STT3B also led to a small but reproducible reduction in cotranslational N-glycosylation of the NFT site (Figure 4B, top right panel). Although experimentally significant (Table 1 of the Supporting Information), the STT3B-linked reduction in cotranslational N-glycosylation likely stems from our simplified definition (the zero time point), which for the NFT site, is likely (compared to the NFS site) to contain faster post-translational events that occur during the 2 min pulse (*vide infra*). If we exclude the NFT site anomaly, our results with type I transmembrane peptides are consistent with previous findings, where STT3A modifies N-linked consensus sites cotranslationally and STT3B modifies the skipped consensus sites post-translationally.

The recently determined eubacterial and aracheal OST homologue structures[9,10] afford an opportunity to glean a structural rationale for the effect of the middle X residue on co- and post-translational N-glycosylation. Figure 5 (top left) shows a close-up view of the eubacterial PglB crystal structure[9]

dx.doi.org/10.1021/bi500681p | *Biochemistry* 2014, 53, 4884–4893

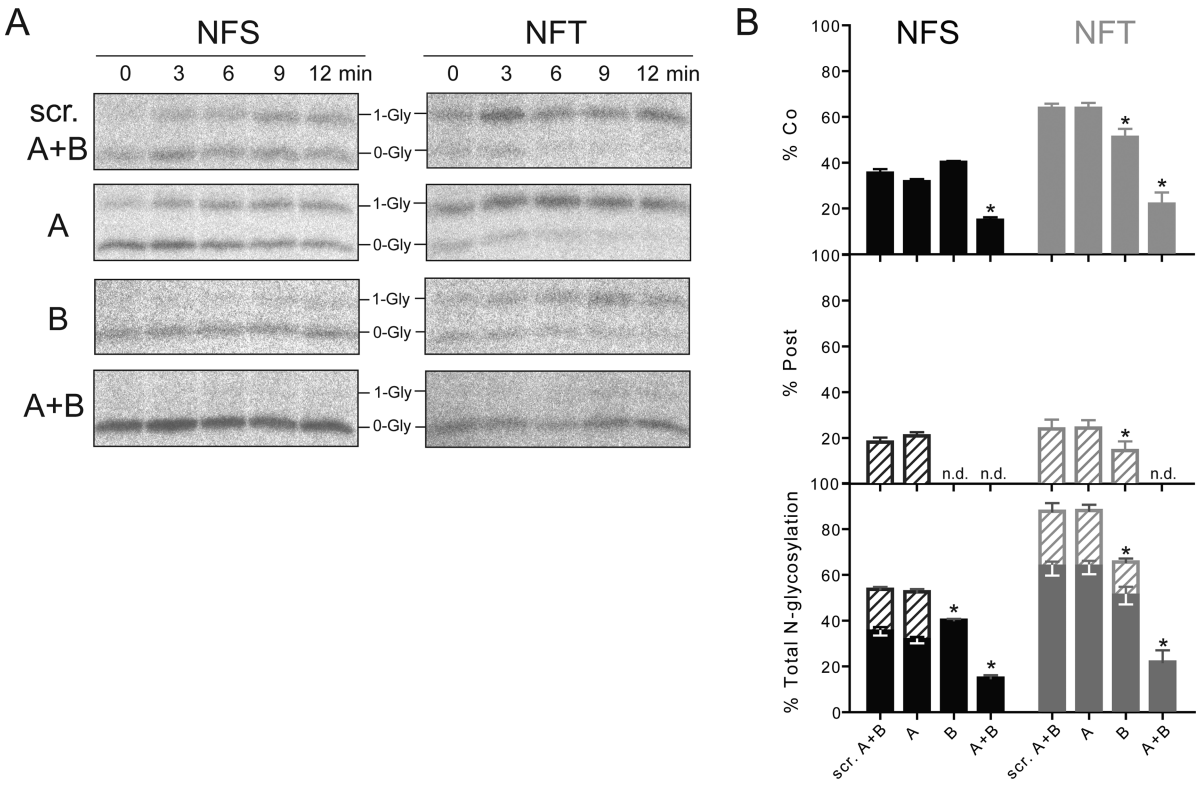

Figure 4. Co- and post-translational N-glycosylation of NXS and NXT sites in type I transmembrane peptides is performed by catalytic OST isoforms STT3A and STT3B, respectively. (A) Representative fluorographs from pulse-chased, siRNA-treated cells expressing either an NFS or NFT site. The STT3 specificity of each siRNA is shown on the left: scrambled STT3A and STT3B (scr. A+B), STT3A (A), STT3B (B), and STT3A and STT3B (A+B). Glycosylated (1-Gly) and unglycosylated (0-Gly) species are labeled. (B) Bar graphs for cotranslational (solid), post-translational (hatched), and total N-glycosylation of NFS (black) and NFT (gray) consensus sites for the different siRNA treatments. All error bars show the standard error of the mean from three experiments; n.d. means not detected. *$p < 0.05$. The errors in the combined bar graph are denoted as follows: cotranslational (middle bar, up), post-translational (middle bar, down), and total N-glycosylation (top bar, up).

in which the peptide substrate containing an NAT consensus site bends to tightly pack within the peptide recognition site of the enzyme. Using PyMOL, we substituted middle X residues and visually inspected each rotamer for steric and electrostatic clashes (Experimental Procedures). The remaining panels in Figure 5 depict the wild-type structure and middle X residue rotamers with minimal steric clashes for the most efficiently glycosylated site (cysteine), oppositely charged residues (arginine and glutamic acid), and the worst consensus site (tryptophan). Although definitive conclusions using a static structure are limited and lack any kinetic information about the binding site interactions, substituting the middle X residue into the structure provides a qualitative picture of the molecular gyrations needed to accommodate the differently charged and sized amino acid side chains. In all of the panels, the middle X residue α-carbon sits just below three PglB bottleneck residues: N55, D465, and M318 (Figure 5). In the crystal structure, the alanine side chain sits squarely in the pocket consisting of these three PglB residues. When alanine is mutated to cysteine, almost all rotamers effectively maneuver around this bottleneck, and polar residues have the potential to form hydrogen bonds with PglB residue N55 or D465. In contrast, large hydrophobic residues have very few rotamers in which steric clashes do not exist and tryptophan cannot be accommodated in any rotamer (Figure 5), highlighting the intolerance of bulky side chains in this constrained region.

Most rotamers of the charged residues (Figure 5, Arg and Glu) avoid the PglB bottleneck by extending their side chains into a larger cavity between the polar (N55) and negatively charged (D465) side chains of PglB, which may explain why negatively charged NXS sites are less efficiently N-glycosylated. On the basis of sequence alignments with the mammalian OST STT3A and STT3B isoforms, N55 is predicted to be a glutamic acid and serine, respectively; D465 is part of the conserved WWD sequence that is thought to form a hydrogen bond to the hydroxyl residue of the consensus site.[9] Thus, the greater negative charge in the STT3A pocket may underlie the subtle differences we observed between co- and post-translational N-glycosylation of the similarly charged (i.e., D vs E or R vs K) residues (Figure 3C). Although PglB is a prokaryotic homologue that modifies a slightly different consensus sequence,[22] its peptide binding site provides a structural basis for the mammalian OST co- and post-translational N-glycosylation kinetics of the different NXS consensus sites.

DISCUSSION

Previous studies have shown that N-glycan efficiency is influenced by the middle X residue in NXS, but not NXT sites. Here, we determined the kinetic and enzymatic basis for the effect of the X residue on N-glycosylation efficiency. Using rapid pulse−chase experiments with a type I transmembrane peptide model substrate expressed in N-glycosylation proficient cells, we found a wide range of cotranslational efficiencies (~15−85%) for NXS consensus sites. In general, consensus sites containing large hydrophobic residues (W, L, F, I, and M) and glutamic acid were skipped (>50%) by the OST during

dx.doi.org/10.1021/bi500681p | Biochemistry 2014, 53, 4884−4893

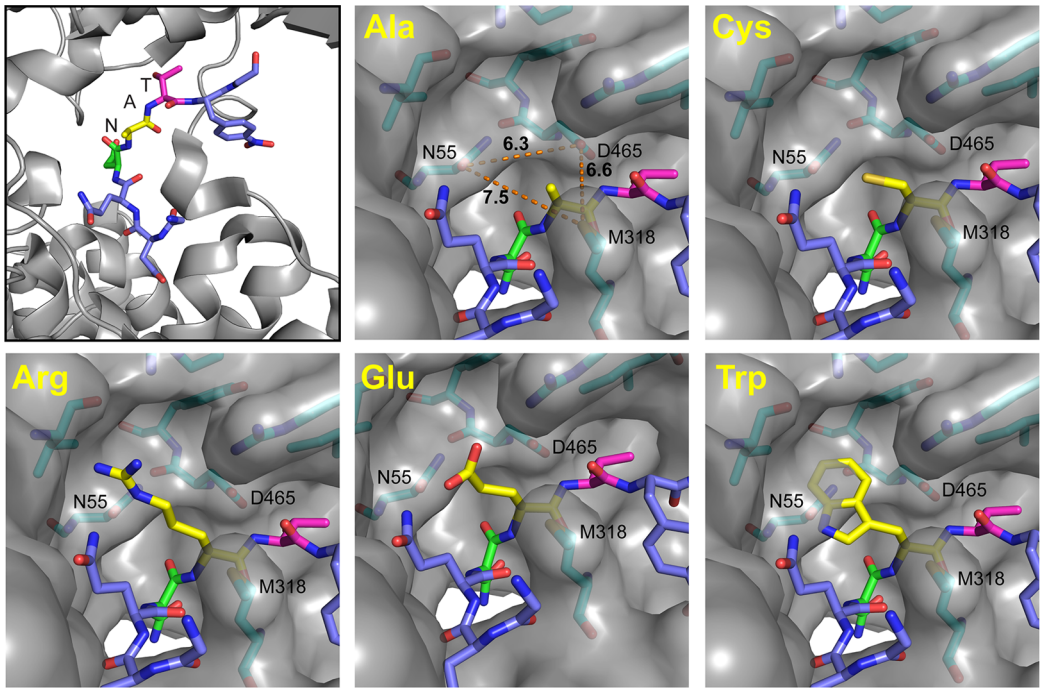

Figure 5. Models of middle X residues in the PglB oligosaccharyltransferase crystal structure. The top left panel shows a close-up view of the bent NAT consensus site peptide in the PglB peptide binding site (PDB entry 3RCE):[9] N, green; A, yellow; T, pink. The remaining panels show NXT consensus site peptide models for middle X residues with various N-glycosylation efficiencies. The middle X residue in the crystal structure (Ala) was mutated, and a rotamer with no steric clashes is shown for each mutant except tryptophan, which cannot be positioned without introducing a steric clash. The three PglB residues (N55, D465, and M318) that surround the consensus site middle X residue are denoted. Numbers in the alanine panel are given in angstroms.

translation whereas small and polar residues were the most efficiently modified. For NXS sites that acquire the majority of their N-glycans during translation, post-translational N-glycosylation effectively modified the skipped sites, yielding 80−95% glycosylated protein (Table 1). However, the post-translational N-glycosylation machinery cannot compensate for severe cotranslational inadequacies; thus, the worst NXS sites, in particular NWS and NLS, remain hypoglycosylated at the end of the time course. For the corresponding NXT sites, the addition of the methyl group to the consensus site significantly improved cotranslational N-glycosylation, completely ameliorating the effect of the X residue on all consensus sites except NWT, which requires post-translational N-glycosylation to yield ∼70% glycosylated protein.

For the most part, our kinetic investigation of the consensus site middle X and hydroxyl residues is in harmony with previous *in vitro* glycosylation efficiency studies:[11−14] large hydrophobic and negatively charged middle X residues in NXS sites are poorly glycosylated, and conversion to NXT significantly improves their overall N-glycosylation efficiency. However, on an amino acid by amino acid basis, there are subtle differences. The most noticeable is that negatively charged X residues are poorly glycosylated *in vitro*,[13] whereas in our cell-based system, NES and NDS have efficiencies comparable to those of the intermediately modified hydrophobic NXS consensus sites (NMS, NIS, and NFS). Given that two different substrates and assays were used, the congruence of the results indicates that the effect of the middle X residue on NXS sites (and lack thereof on NXT sites) is general and does not depend on the protein substrate.

The rapid pulse−chase experiments also allowed us to determine whether co- and post-translational N-glycosylation were equally affected by the middle X and hydroxyl residues (Figure 3 and Table 1). Although the measured k_{obs} values for the individual NXS sites were not significantly different from each other (Table 1), a significant correlation between co- and post-translational N-glycosylation was observed (Figure 3). In addition, switching the consensus site hydroxyl group from serine to threonine also improved co- and post-translational N-glycosylation similarly, yielding more cotranslational N-glycosylation and concomitantly increasing k_{obs} such that the level of post-translational N-glycosylation was significantly increased for NET and measurable for NWT and NLT (Table 1). Together, these data suggest that co- and post-translational N-glycosylation machineries utilize a conserved N-glycan attachment mechanism that is similarly affected by consensus site X and hydroxyl residues. Thus, both co- and post-translational N-glycosylation underlie the NXS and NXT N-glycosylation efficiencies previously observed in *in vitro* translation assays.[11−14]

Because the consensus site middle X and hydroxyl residues similarly affected N-glycan attachment during and after translation, we used RNAi to identify the OST STT3 isoforms responsible for co- and post-translational N-glycosylation of these type I transmembrane peptide substrates. As in previous studies with water-soluble and type II transmembrane peptides,[5,7] we found that STT3A predominantly performs cotranslational N-glycosylation whereas STT3B predominantly performs post-translational N-glycosylation and will perform cotranslational modifications in the absence of STT3A (Figure 4).

Curiously, the STT3B knockdown also significantly reduced cotranslational N-glycosylation of the NFT substrate (Figure 4 and Table 1 of the Supporting Information). Given that it is

dx.doi.org/10.1021/bi500681p | *Biochemistry* 2014, 53, 4884−4893

unlikely that the STT3B isoform is specifically modifying the NFT, but not the NFS construct during protein translation, we attribute this apparent reduction in cotranslational N-glycosylation to post-translational (STT3B) events occurring during the zero time point because the type I transmembrane substrates are small (~150 amino acids), spend approximately 10 s in the ER translocon during translation of the C-terminus,[23] and require a 2 min pulse to achieve experimentally tractable amounts of radiolabeled protein. For comparsion, hemagglutinin, which is twice the size of the constructs used in our study, is readily detected ~1 min after radiolabel treatment of CHO cells.[21] Thus, any consensus sites that are skipped during translation can be modified post-translationally during the pulse period. Because NFT sites are post-translationally modified twice as fast as NFS sites, the NFT zero time point will contain more STT3B modifications, which is what was observed in the OST knockdown experiments (Figure 4B).

In contrast, we do not expect the chase time points (3−12 min) to be contaminated with any cotranslational events because of the rapid (<1 min) depletion of the metabolic radiolabel that has been observed during chase times using proteins with evenly distributed methionines.[21] Moreover, our methionine-poor type I transmembrane substrates are intentionally "back loaded" with five methionines in the C-terminus such that any partially synthesized proteins will have minimal radioactive signals when chased with cold media. A less precise measurement of cotranslational but not the post-translational events predicts that the most efficiently N-glycosylated consensus sites will have an artificially higher cotranslational N-glycosylation efficiency when compared to their post-translational rates. The data in Figure 3C are consistent with this prediction, as the highly efficient polar X residues cluster above and to the left of the linear trend. In addition, a similar shift is observed for the other KCNE type I transmembrane peptides where the more efficiently N-glycosylated consensus sites cluster higher and to the left of the fit (Figure 3 of the Supporting Information). Overall, our knockdown studies with type I transmembrane peptides are consistent with the previous co- and post-translational roles assigned to the OST STT3A and STT3B isoforms and further underscore the importance of post-translational N-glycosylation of NXS and NXT consensus sites skipped during protein translation.

Utilizing the known eubacterial STT3 homologue structure PglB, we gleaned a potential structural explanation for the spectrum of kinetic rates observed for different X residues in consensus sites (Figure 5). A conserved bottleneck of PglB residues around the middle X residue in the peptide recognition site may account for limitations in N-glycan attachment efficiency for larger hydrophobic residues, where significant rearrangement is required to accommodate the more voluminous side chains. To fully elucidate the molecular nuances associated with co- and post-translational consensus site recognition, future high-resolution structures and/or computational docking studies with various NXS and NXT consensus sites are needed.

This study adds to the previously identified molecular determinants[20] of co- and post-translational N-glycosylation of the KCNE family of type I transmembrane peptides, where mutations that shift the kinetics of N-glycosylation give rise to cardioauditory diseases.[19] Previously, we could not adequately explain why co- and post-translational N-glycosylation of KCNE5 consensus sites did not strongly depend on the consensus site hydroxyl group.[20] A retrospective glance at the KCNE5 consensus sites suggests that this discrepancy is due to the middle X residues, which are cysteine and alanine, two of the most efficiently cotranslationally N-glycosylated NXS sites. This implies that KCNE5, unlike the other KCNE peptides that contain mostly NXT sites, evolved an efficient middle X residue versus a more efficient hydroxyl residue and implicates multiple avenues of evolution to ensure a high N-glycan occupancy rate. In evidence, post hoc analysis[a] of a recent computational study[24] showed that among middle X residues in mouse glycoprotein consensus sites determined to by occupied *in vivo*, cysteine is overrepresented.

Examination of the middle X and hydroxyl residues in previous studies utilizing water-soluble and membrane proteins also suggests that our results with a type I transmembrane peptide scaffold may be general for all full-length proteins. The middle X residues in these post-translationally identified consensus sites[4,6,25,26] were leucine, phenylalanine, isoleucine, and aspartic acid, the consensus sites most frequently skipped by the cotranslational machinery (STT3A) in our study. Moreover, all of the post-translational consensus sites in these prior studies contained a serine hydroxyl residue, except for consensus sites located at the extreme C-terminus of the protein[7] and factor VII.[4] These exceptions underscore the need for future studies that carefully define the molecular determinants important for co- and post-translational N-glycosylation of NXS and NXT consensus sites in other topologically distinct transmembrane peptides, polytopic membrane proteins, and water-soluble proteins.

■ ASSOCIATED CONTENT

Supporting Information

Additional observations. This material is available free of charge via the Internet at http://pubs.acs.org.

■ AUTHOR INFORMATION

Corresponding Author

*Department of Biochemistry and Molecular Pharmacology, University of Massachusetts Medical School, 364 Plantation St., Worcester, MA 01605-2324. E-mail: william.kobertz@umassmed.edu. Phone: (508) 856-8861. Fax: (508) 856-8867.

Author Contributions

H.L.H.M. and W.R.K. designed the experiments and wrote the manuscript. H.L.H.M. performed all of the experiments and data analysis.

Funding

This work was supported by a grant to W.R.K. from the National Institutes of Health (GM-070650).

Notes

The authors declare no competing financial interest.

■ ACKNOWLEDGMENTS

We thank Drs. Reid Gilmore and Natalia Cherepanova for the siRNA sequences for targeting STT3A and STT3B in CHO cells.

■ ABBREVIATIONS

OST, oligosaccharyltransferase; ER, endoplasmic reticulum; E1−E5, KCNE1−KCNE5, respectively.

■ ADDITIONAL NOTE

[a]Unpublished data from R. Gilmore (University of Massachusetts Medical School) by personal communication.

REFERENCES

(1) Silberstein, S., and Gilmore, R. (1996) Biochemistry, molecular biology, and genetics of the oligosaccharyltransferase. *FASEB J. 10*, 849−858.

(2) Mohorko, E., Glockshuber, R., and Aebi, M. (2011) Oligosaccharyltransferase: The central enzyme of N-linked protein glycosylation. *J. Inherited Metab. Dis. 34*, 869−878.

(3) Shao, S., and Hegde, R. S. (2011) Membrane protein insertion at the endoplasmic reticulum. *Annu. Rev. Cell Dev. Biol. 27*, 25−56.

(4) Bolt, G., Kristensen, C., and Steenstrup, T. D. (2005) Posttranslational N-glycosylation takes place during the normal processing of human coagulation factor VII. *Glycobiology 15*, 541−547.

(5) Ruiz-Canada, C., Kelleher, D. J., and Gilmore, R. (2009) Cotranslational and posttranslational N-glycosylation of polypeptides by distinct mammalian OST isoforms. *Cell 136*, 272−283.

(6) Suzuki, S., Shuto, T., Sato, T., Kaneko, M., Takada, T., Suico, M. A., Cyr, D. M., Suzuki, H., and Kai, H. (2014) Inhibition of post-translational N-glycosylation by HRD1 that controls the fate of ABCG5/8 transporter. *Sci. Rep. 4*, 4258.

(7) Shrimal, S., Trueman, S. F., and Gilmore, R. (2013) Extreme C-terminal sites are posttranslocationally glycosylated by the STT3B isoform of the OST. *J. Cell Biol. 201*, 81−95.

(8) Kelleher, D. J., and Gilmore, R. (2006) An evolving view of the eukaryotic oligosaccharyltransferase. *Glycobiology 16*, 47R−62R.

(9) Lizak, C., Gerber, S., Numao, S., Aebi, M., and Locher, K. P. (2011) X-ray structure of a bacterial oligosaccharyltransferase. *Nature 474*, 350−355.

(10) Matsumoto, S., Shimada, A., Nyirenda, J., Igura, M., Kawano, Y., and Kohda, D. (2013) Crystal structures of an archaeal oligosaccharyltransferase provide insights into the catalytic cycle of N-linked protein glycosylation. *Proc. Natl. Acad. Sci. U.S.A. 110*, 17868−17873.

(11) Breuer, W., Klein, R. A., Hardt, B., Bartoschek, A., and Bause, E. (2001) Oligosaccharyltransferase is highly specific for the hydroxy amino acid in Asn-Xaa-Thr/Ser. *FEBS Lett. 501*, 106−110.

(12) Bause, E., and Legler, G. (1981) The role of the hydroxy amino acid in the triplet sequence Asn-Xaa-Thr(Ser) for the N-glycosylation step during glycoprotein biosynthesis. *Biochem. J. 195*, 639−644.

(13) Shakin-Eshleman, S. H., Spitalnik, S. L., and Kasturi, L. (1996) The amino acid at the X position of an Asn-X-Ser sequon is an important determinant of N-linked core-glycosylation efficiency. *J. Biol. Chem. 271*, 6363−6366.

(14) Kasturi, L., Chen, H., and Shakin-Eshleman, S. H. (1997) Regulation of N-linked core glycosylation: Use of a site-directed mutagenesis approach to identify Asn-Xaa-Ser/Thr sequons that are poor oligosaccharide acceptors. *Biochem. J. 323* (Part2), 415−419.

(15) Ben-Dor, S., Esterman, N., Rubin, E., and Sharon, N. (2004) Biases and complex patterns in the residues flanking protein N-glycosylation sites. *Glycobiology 14*, 95−101.

(16) Igura, M., and Kohda, D. (2011) Quantitative assessment of the preferences for the amino acid residues flanking archaeal N-linked glycosylation sites. *Glycobiology 21*, 575−583.

(17) Mellquist, J. L., Kasturi, L., Spitalnik, S. L., and Shakin-Eshleman, S. H. (1998) The amino acid following an Asn-X-Ser/Thr sequon is an important determinant of N-linked core glycosylation efficiency. *Biochemistry 37*, 6833−6837.

(18) Shrimal, S., and Gilmore, R. (2013) Glycosylation of closely spaced acceptor sites in human glycoproteins. *J. Cell Sci. 126*, 5513−5523.

(19) Bas, T., Gao, G. Y., Lvov, A., Chandrasekhar, K. D., Gilmore, R., and Kobertz, W. R. (2011) Post-translational N-glycosylation of type I transmembrane KCNE1 peptides: Implications for membrane protein biogenesis and disease. *J. Biol. Chem. 286*, 28150−28159.

(20) Malaby, H. L., and Kobertz, W. R. (2013) Molecular determinants of co- and post-translational N-glycosylation of type I transmembrane peptides. *Biochem. J. 453*, 427−434.

(21) Braakman, I., Hoover-Litty, H., Wagner, K. R., and Helenius, A. (1991) Folding of influenza hemagglutinin in the endoplasmic reticulum. *J. Cell Biol. 114*, 401−411.

(22) Kowarik, M., Young, N. M., Numao, S., Schulz, B. L., Hug, I., Callewaert, N., Mills, D. C., Watson, D. C., Hernandez, M., Kelly, J. F., Wacker, M., and Aebi, M. (2006) Definition of the bacterial N-glycosylation site consensus sequence. *EMBO J. 25*, 1957−1966.

(23) Hershey, J. W. (1991) Translational control in mammalian cells. *Annu. Rev. Biochem. 60*, 717−755.

(24) Zielinska, D. F., Gnad, F., Wisniewski, J. R., and Mann, M. (2010) Precision mapping of an in vivo N-glycoproteome reveals rigid topological and sequence constraints. *Cell 141*, 897−907.

(25) Kolhekar, A. S., Quon, A. S., Berard, C. A., Mains, R. E., and Eipper, B. A. (1998) Post-translational N-glycosylation of a truncated form of a peptide processing enzyme. *J. Biol. Chem. 273*, 23012−23018.

(26) Sato, T., Sako, Y., Sho, M., Momohara, M., Suico, M. A., Shuto, T., Nishitoh, H., Okiyoneda, T., Kokame, K., Kaneko, M., Taura, M., Miyata, M., Chosa, K., Koga, T., Morino-Koga, S., Wada, I., and Kai, H. (2012) STT3B-dependent posttranslational N-glycosylation as a surveillance system for secretory protein. *Mol. Cell 47*, 99−110.